metals

MDPI

Article

Analysis and Investigation of Trilateral Spinning Based on the Concentric Circle Trajectory

Xibin Ou [1], Xianyong Zhu [1,*], Peng Gu [2], Baichao Wang [3], Jinsong Liu [2] and Song Yang [1]

[1] School of Mechanical and Aerospace Engineering, Jilin University, Changchun 130025, China; ouxb17@mails.jlu.edu.cn (X.O.); yangsongjlu@jlu.edu.cn (S.Y.)
[2] Changchun Equipment & Technology Research Institute, Changchun 130012, China; gupeng521_cngc@163.com (P.G.); liujinsong_cngc@163.com (J.L.)
[3] College of Mechanical and Electrical Engineering, Changchun University of Science and Technology, Changchun 130022, China; bcwang@cust.edu.cn
* Correspondence: zhuxy@jlu.edu.cn; Tel.: +86-130-1920-7121

Abstract: Several researchers have developed various spinning methods to produce non-circular hollow parts. In this paper, an approach that the rollers revolve around the roller principal axis was used to generate a concentric circular trajectory to the spinning trilateral workpiece. The spinning simulation was performed in ABAQUS 2016/Explicit software. The trajectory of the roller is derived, and the distributions of the equivalent von Mises stress, equivalent strain, wall thickness of the workpiece in typical section and spinning force are obtained. The simulation experiment proves the feasibility of using the proposed spinning method to produce workpieces with trilateral cross-section. The results demonstrated that after seven passes, in the area where the roller unloads the workpiece and the area where the roller starts the forward pass, local wrinkling may be generated; the most vulnerable area of the workpiece is also located at the area where the roller starts the forward pass, while the overall thinning rate of the workpiece is below 21%. Compared with other existent non-circular spinning methods, this novel method could process non-circular parts with a high rotational velocity, while ensuring the roller processing trajectory with high accuracy. The application of this method will improve the efficiency of the process by more than 200% in theory, while ensuring workpiece quality

Keywords: non-circular spinning; FE model; concentric circle trajectory; spinning quality

check for updates

Citation: Ou, X.; Zhu, X.; Gu, P.; Wang, B.; Liu, J.; Yang, S. Analysis and Investigation of Trilateral Spinning Based on the Concentric Circle Trajectory. *Metals* **2022**, *12*, 647. https://doi.org/10.3390/met12040647

Academic Editor: Badis Haddag

Received: 21 February 2022
Accepted: 7 April 2022
Published: 11 April 2022

Publisher's Note: MDPI stays neutral with regard to jurisdictional claims in published maps and institutional affiliations.

Copyright: © 2022 by the authors. Licensee MDPI, Basel, Switzerland. This article is an open access article distributed under the terms and conditions of the Creative Commons Attribution (CC BY) license (https://creativecommons.org/licenses/by/4.0/).

1. Introduction

Metal spinning is a plastic forming method, where a flat metal blank or prefabricated blank is rotated around the principal axis, while rollers apply pressure on the blank, producing continuous and point-by-point plastic deformation until a hollow workpiece is obtained. Due to its high material utilization and low cost, metal spinning is widely used in the aerospace, automobile, military, and other industries [1–5]. The spinning technology has been used for a long time to produce hollow parts with circular cross-section. In recent years, non-circular spinning has become one of the frontier research areas in the field. Several scholars have also succeeded in spin non-circular workpieces through various methods.

In general, there are two ways to achieve non-circular spinning: (1) synchronous spinning; and (2) force-controlled spinning.

In synchronous spinning, the rotation angle of the workpiece is synchronized with the radial feed of the roller. To produce a workpiece with elliptical cross-section, Amano and Tamura [6] developed a mechanism composed of cams and links, by which the rollers followed an elliptical track to spin the blank. This research proved for the first time that the spinning technology could produce non-circular parts as well. Gao et al. [7,8] used a method contrary to that of Amano and Tamura, where the three-jaw chuck was installed

on two orthogonal sliding chutes enabling the workpiece to follow an elliptical track, and an elliptical head and cone were obtained. It should be mentioned that early-phase non-circular methods were basically limited to elliptical spinning.

More recently, Xia et al. [9–11] developed a spinning device for non-circular cross-sections based on the profiling driving spinning method and they obtained several types of regular non-circular hollow parts, such as triangles, quadrilaterals, and pentagons. Shimizu [12] developed a non-circular spinning device, where a stepping motor controlled the rotation of a mandrel, while electric actuators controlled the radial feed of the roller and the axial movement of the workpiece. The device produced asymmetric truncated-elliptical-cone-shaped products with a sidewall, as well as truncated-pyramid-shaped products.

Jia et al. [13–16] used a synchronous spinning method to produce hollow parts with non-circular cross-section on a computer numerical controlled (CNC) spinning machine without using a mandrel. The spinning path for producing non-circular cones was optimized mathematically. Sugitaa and Arai [17–19] used synchronous multi-pass spinning to produce workpieces with non-circular bottom and vertical walls. In another study, Härtel and Laue [20] formed a tripod workpiece based on a spinning equipment with a two-axes table for radial and axial feed of the roller, and they used the numerical simulation method to research on optimizing the workpiece quality. In a later study, Aria and Kanazawab [21] used synchronous multi-pass spinning to produce a square cup-shaped workpiece with inclined bottom and vertical side walls and they formed an intermediate circular shape to make the wall thickness even.

In force-controlled spinning, a non-circular workpiece is processed by controlling the spinning force to ensure the rollers can press firmly on the blank to complete spinning. Arai [22] produced parts with polygonal cross-section by force-controlled spinning. He developed a device where ball screws and servo motors drive the axial and radial feed of the roller, and the mandrel is rotated by a servo motor. A force sensor placed behind the roller sends feedback to a computer which sends commands to the servo motors to apply the required force. To produce triangular-shaped hollow parts, Awiszus and Meyer [23] developed a method using springs to force two rollers to pull each other and fit the workpiece over a non-circular mandrel. In another research, Arai [24] employed a linear servo motor to drive the roller, which accelerated the reaction time of the roller radial feed during spinning and improved the non-circular spinning efficiency.

In this paper, a novel method is proposed to process non-circular parts with a high rotational velocity, while ensuring a high accuracy of roller processing trajectory. It means that the application of this method will improve the efficiency of spinning non-circular parts and guarantee the quality of the parts. We researched on forming trilateral non-circular workpieces which is the most difficult processing in the non-circular spinning. In the spinning, three rollers are evenly arranged in the circumferential direction of the center of the roller principal axis, only the angular velocity of the roller principal axis is proportional to the angular velocity of the workpiece, which condition is easily to achieve, then trilateral workpieces would be obtained efficiently with an acceptable quality. Compared with other existent non-circular spinning methods, this novel method avoids the inaccurate trajectory in the method of force-controlled spinning which is because the signal this method controls is the force not the trajectory. It also avoids the low-effectiveness in the method of synchronous spinning, which is because the radial feed of the rollers needs to be synchronized with the rotation angle of the workpiece. In summary, this research provides a novel method for spinning trilateral non-circular workpieces with high-efficiency and high-quality.

2. Methodology

2.1. Finite Element Model Development

Figure 1 shows the 3D FE model trilateral non-circular spinning model. The simulation was performed in ABAQUS 2016/Explicit software. To shorten the duration of the simulation experiment without affecting the results, we employed the technique of equivalent

transformation [25–27]. The motion of the rollers rotated around the roller principal axis to process the workpiece, which rotated itself, was set as the workpiece static, the roller principal axis revolved around the workpiece, while the rollers revolved around the roller principal axis.

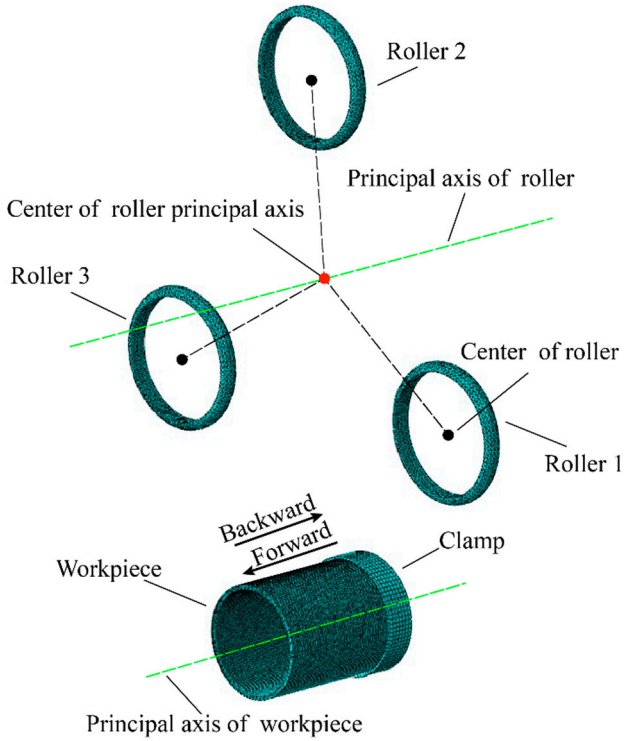


Figure 1. Finite element model of the trilateral non-circular spinning configuration.

In the 3D FE model, the three rollers and the clamp were defined as rigid bodies, while the workpiece was defined as a deformable part. The element type of the workpiece is 8-node hexahedral linear reduced-integration element (C3D8R) for the simulation. The position of the clamp was fixed. The distance between the center of each roller and the roller principal axis was 150 mm, and the three rollers were circumferentially installed and evenly distributed at an interval of 120°. The inner surface of the clamp was connected with one end of the workpiece using the tie function. Thus, the area where the workpiece is connected with the clamp was constrained during the spinning process. The rest of the workpiece was free to deform during spinning. The center of the roller principal axis was connected with the center of each roller using the hinge function. The workpiece had a diameter of 80 mm, thickness of 3 mm, and total length of 110 mm. To improve the simulation efficiency while maintaining the accuracy of the results, the constrained parts and free parts of the workpiece were meshed differently. More specifically, the free part of the workpiece was meshed with elements 1.25 mm in length along the axial direction and 0.75 mm along the thickness direction, while the angle between the two sides of the mesh was 1.8° in circumferential directions. The constrained part of the workpiece was meshed with elements 2 mm in length along the axial direction, while the other two dimensions were the same as those in the free part. In total, there were 70,752 elements and 89,445 nodes. The material of the workpiece was set as 6061-aluminum alloy, and the isotropic elasto-plasticity material model was used for it. The material properties are listed in Table 1. The relationship of the true stress and strain was $Y = 229.88 \in^{0.25}$, and the Coulomb friction coefficient between the workpiece and the rollers was set to 0.1 [28,29].

Table 1. Mechanical properties of the 6061-aluminum alloy.

Mechanical Properties	Value
Yield strength	62.05 MPa
Ultimate strength	151.68 MPa
Young's modulus	69,000 MPa
Poisson's ratio	0.3

2.2. Roller Trajectory Equation Analysis

When the rollers revolve around the center of the roller principal axis, trilateral non-circular hollow parts can be processed through two different methods. One method can be based on the hypocycloid principle. The definition of the hypocycloid can be seen in Figure 2, where a moving circle is inscribed into a fixed circle, and the moving circle rolls along the fixed one without sliding; then, the trajectory of any point on the moving circle is a hypocycloid. If the radius of the fixed circle is R, the radius of the moving circle is r, and a point P is fixed on the moving circle, then the trajectory of point P can be determined by the hypocycloid equation [30–32]:

$$\begin{cases} x = (R-r)\cos\theta + r\cos\frac{R-r}{r}\theta \\ y = (R-r)\sin\theta - r\sin\frac{R-r}{r}>\theta \end{cases} \quad (-\infty < \theta < +\infty) \tag{1}$$

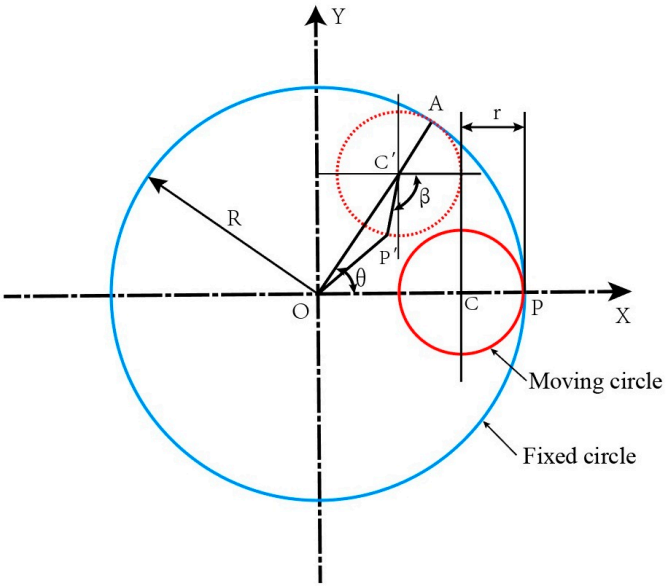


Figure 2. Schematic illustration of the roller trajectory.

When $R = 3r$, the hypocycloid equation becomes:

$$\begin{cases} x = 2R\cos\theta + r\cos 2\theta \\ y = 2Rsin\theta - rsin2\theta \end{cases} \quad (-\infty < \theta < +\infty) \tag{2}$$

The trajectory produced by Equation (2) is shown in Figure 3. If the roller is modeled as point P, the trajectory of the roller is a triangle composed of three concave curves. Awiszus and Meyer [23] indicated that non-circular parts with three-concave-curve cross-sections are prone to defects such as wrinkles. Therefore, in this research, a different method, where the rollers revolve around the center of the roller principal axis, was used to process the triangular non-circular workpiece.

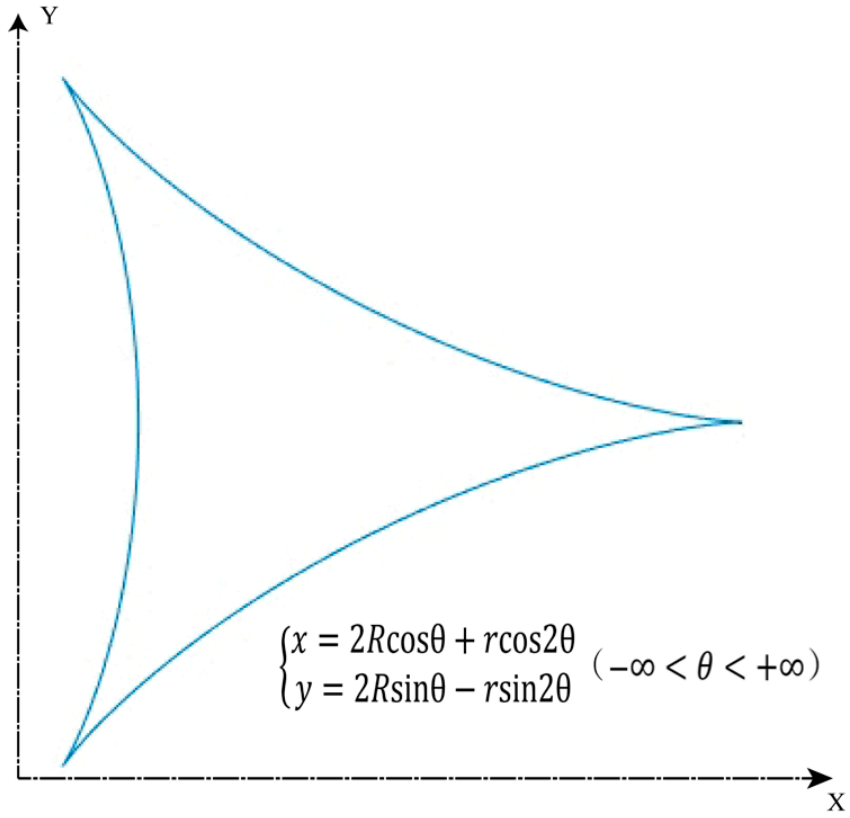


Figure 3. Trajectory produced by Equation (2).

In order to prove the effectiveness of the alternative method, the trajectory of the rollers relative to the workpiece should be identified first. As mentioned above, the spinning process where the rollers revolve around the center of the roller principal axis while the workpiece rotates about itself can be transformed into a process where the workpiece is stationary, and the roller principal axis revolves around the workpiece while the rollers revolve around the center of the roller principal axis. Consequently, as shown in Figure 2, the roller is modeled as a fixed point P on the moving circle with center C and radius r. The moving circle is inscribed into a fixed circle with center O and radius R. The unit vector in the horizontal x-axis is $\vec{\imath}$ and that in the vertical y-axis is $\vec{J}$. At the beginning, the point P coincides with the x-axis. Subsequently, the center of the moving circle starts to revolve counterclockwise around the center of the fixed circle at an angular velocity of ω rad/s, and the moving circle rotates clockwise at φ rad/s. After t seconds, the center of the moving circle C moves to C′ and point P moves to P′, as a result:

$$\overrightarrow{OP'} = \overrightarrow{OC'} + \overrightarrow{C'P'} \tag{3}$$

If

$$\theta = \measuredangle\left(\vec{\imath}, \overrightarrow{OC'}\right) = \omega t, \beta = \measuredangle\left(\vec{\imath}, \overrightarrow{C'P'}\right) = -\varphi t \tag{4}$$

Then

$$\overrightarrow{OC'} = \vec{\imath}(R-r)\cos\theta + \vec{J}(R-r)\sin\theta = \vec{\imath}(R-r)\cos\omega t + \vec{J}(R-r)\sin\omega t \tag{5}$$

$$\overrightarrow{C'P'} = \vec{\imath}\,\mathrm{r}\cos(-\varphi t) + \vec{J}\,\mathrm{r}\sin(-\varphi t) \tag{6}$$

$$\begin{aligned}\overrightarrow{OP'} &= \overrightarrow{OC'} + \overrightarrow{C'P'} = \vec{i}(R-r)\cos\omega t + \vec{J}(R-r)\sin\omega t + \vec{i}\,r\cos(-\varphi t) + \vec{J}\,r\sin(-\varphi t) \\ &= \vec{i}\left((R-r)\cos\omega t + r\cos(-\varphi t)\right) + \vec{J}\left((R-r)\sin\omega t + r\sin(-\varphi t)\right)\end{aligned} \tag{7}$$

Therefore, the coordinates of point P at any time t are:

$$\begin{cases} x = (R-r)\cos\omega t + r\cos(-\varphi t) \\ y = (R-r)\sin\omega t + r\sin(-\varphi t) \end{cases} \tag{8}$$

Then

$$\begin{cases} x = (R-r)\cos\omega t + r\cos(\varphi t) \\ y = (R-r)\sin\omega t - r\sin(\varphi t) \end{cases} \tag{9}$$

Especially when $\varphi = 0$, the coordinates of point P at any time t are:

$$\begin{cases} x = (R-r)\cos\omega t + r \\ y = (R-r)\sin\omega t \end{cases} \tag{10}$$

Then, if $\theta = \omega t$:

$$\begin{cases} x = (R-r)\cos\theta + r \\ y = (R-r)\sin\theta \end{cases} \tag{11}$$

This means that the coordinates of point P are a circle which its center at (r,0) and radius is $(R - r)$.

2.3. Theory of Trilateral Non-Circular Spinning

According to the above analysis, when φ = 0, it means that the angular velocity of the center of the roller principal axis revolving around the workpiece is equal to the angular velocity of the roller revolving around the center of the roller principal axis, and the trajectory of the roller relative to the workpiece is a circle which has its center at (r,0) and radius is $(R - r)$. Although the radius of the fixed circle R would change, the circle center of the roller trajectory relative to the workpiece remains unchanged, since it is a set of concentric circles. Consequently, to produce a workpiece with triangular cross-section, three rollers are evenly arranged circumferentially around the center of the roller principal axis at an interval of 120° as shown in Figure 2. The trajectory equations of the three rollers are:

$$\begin{cases} x = (R-r)\cos\omega t + r \\ y = (R-r)\sin\omega t \\ x_1 = (R-r)\cos\left(\omega t + \frac{2}{3}\pi\right) - \frac{1}{2}r \\ y_1 = (R-r)\sin\left(\omega t + \frac{2}{3}\pi\right)\omega t + \frac{\sqrt{3}}{2}r \\ x_2 = (R-r)\cos\left(\omega t + \frac{4}{3}\pi\right) - \frac{1}{2}r \\ y_2 = (R-r)\sin\left(\omega t + \frac{4}{3}\pi\right) - \frac{\sqrt{3}}{2}r \end{cases} \tag{12}$$

In Figure 4, it can be seen that the combined trajectory of the three rollers forms a triangle, which is the processing trajectory of the workpiece. Through the radial movement of the center of the roller principal axis at each pass, the workpiece is gradually transformed into the required triangle.

Based on the above theory, it can be found that, in the novel trilateral non-circular spinning method, the synchronization of the radial feed of roller and the rotation angle of the workpiece does not need to be taken into consideration. Only the angular velocity of the roller principal axis is proportional to that of the workpiece, which is an easier to guarantee condition. Therefore, during the spinning process, the spinning trajectory is more accurate, while the efficiency is significantly improved. More specifically, the angular velocity of the workpiece could be increased from 60–240 to 600 rpm [24], improving the efficiency by more than 2 times.

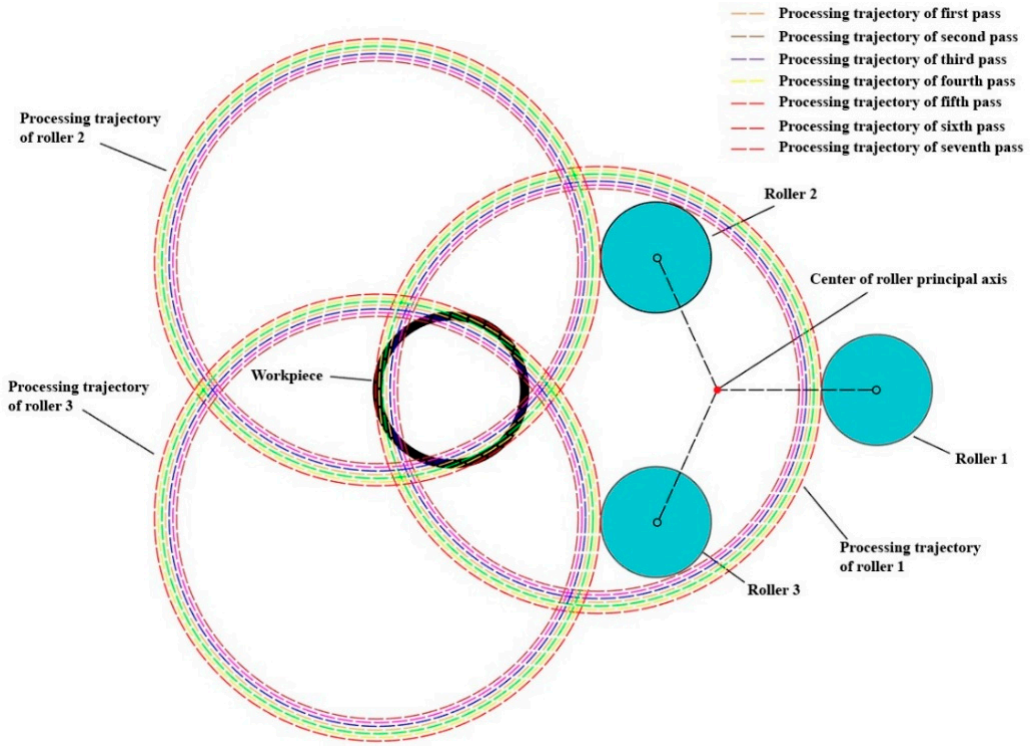


Figure 4. Schematic illustration of the roller trajectories during the spinning of the trilateral workpiece.

2.4. Process Parameter Setting

In the simulation of the trilateral non-circular spinning process, a spinning scheme with multi-pass was adopted which can ensure that the workpiece is formed progressively, while reducing the chances of defects.

In this experiment, there were 7 passes in total. An alternating with forward pass and backward pass adopted (Figure 1), which means that the first, third, fifth, and seventh passes were forward passes, while the second, fourth, and sixth were backward passes.

This alternating pass process can prevent the material flow towards the free end and elongation of the workpiece in the forward pass, which may cause excessive thinning and fracture. It also can avoid the accumulation of material at the head of the roller in the backward pass, which may cause the workpiece to become thicker.

In the first pass, the starting point of spinning is 50 mm away from the fixed end. In the second pass, the stop point is staggered from the starting point of the first pass by 1 mm, which means the stop point is 51 mm away from the fixed end. The starting point of the third pass is staggered by 1 mm from that of the last pass, which means that it is 52 mm away from the fixed end, and so on. The purpose of the staggering is to prevent starting or stopping the spinning at the same position. The undeformed area of the workpiece and the radial feed of the roller would repeatedly pull the workpiece at the same position in each pass, causing excessive thinning and resulting in shrinkage or fracture at this area.

The process parameters for spinning triangular parts mainly include the radial feed of the roller principal axis, the roller diameter, the roller round corner radius, the axial feed of the roller, the angular velocity of the roller principal axis, the angular velocity of the workpiece, and the distance from the center of the roller principal axis to the center of the roller. The process parameters selected in this experiment are given in Table 2.

Table 2. Process parameters selected for simulations.

Parameters	Value
Radial feed of each pass	2 mm, 2 mm, 2 mm, 2 mm, 2 mm, 1 mm, 1 mm
Roller axial feed rate	2 mm/r
Roller round corner radius	6 mm
Angular velocity of the roller principal axis	600 r/min
Angular velocity of the workpiece principal axis	600 r/min
Roller diameter	100 mm
Distance between roller center and center of the roller principal axis	150 mm

3. Results and Discussion

To describe the results clearly, the cross-section of the workpiece was divided into the following stages, as can be seen in Figure 5: the first half loading stage, which is from the roller begins to apply load on the workpiece to the roller at the 0° position; and the second half loading stage, which is from the roller at the 0° position to the roller leaves the workpiece.

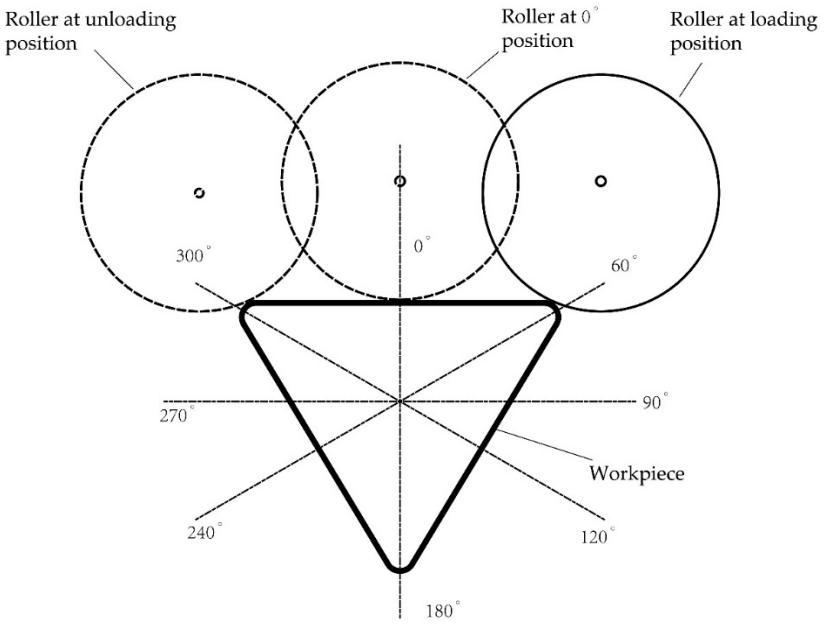


Figure 5. First half loading stage and second half loading stage of the trilateral spinning process.

3.1. Stress Distribution Analysis

3.1.1. Equivalent von Mises Stress Distribution

Figure 6 shows the equivalent von Mises stress distribution on the workpiece after each pass. It can be observed that the stresses developed under this new process did not exhibit layered distribution characteristics. Unlike the traditional spinning method, the roller always exerts spinning force on the workpiece. In the new spinning method, the rollers would alternately load the workpiece and unload the workpiece in the whole process. When the roller is in contact with the workpiece, the workpiece undergoes plastic and elastic deformation. When the roller is separated from the workpiece, the material of the workpiece with elastic strain recovers since the external force exerted by the roller is removed, and thus, the stresses are not evenly distributed. In traditional spinning methods, since the roller and the workpiece are not separated, a stable elasto-plastic strain can be generated; thus, the workpiece may exhibit a layered stress distribution. In the first two passes, the area in the middle of each processed surface exhibited a higher stress

magnitude. Since in the first two passes the initial stage of deformation takes place, the roller exerts relatively higher stress on the workpiece in this area, forcing the cylindrical workpiece to deform. In the area where the roller started the forward pass, which is also the area where the roller stopped spinning after the backward pass, the stress is higher than in other areas. This is due to the fact that the radial feed of the roller principal axis induces the development of tensile stress between the roller and the undeformed area of the workpiece. This tensile stress can pull the material and may lead to excessive thinning, as well as shrinkage or fracture; thus, this is a vulnerable area of the workpiece. After the seventh pass, it can be observed that the stress is more evenly distributed except for the corners of the free end. The even distribution is attributed to the integrity of the workpiece, which results in a uniform stress distribution. The corner stress is because at the free end of the workpiece, the tangential movement of the rollers makes the material flow to the corners, where, after seven passes, a large amount of material is accumulated. Consequently, the roller compresses the accumulated material, generating high levels of stress at the corners.

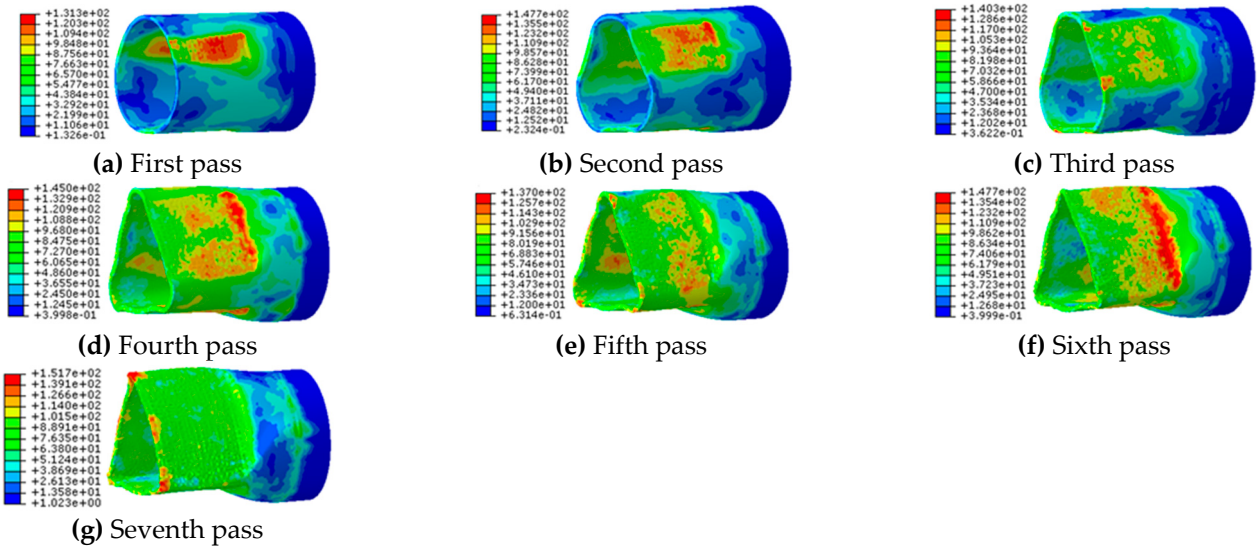


Figure 6. Equivalent von Mises stress distribution after each pass (MPa).

3.1.2. Cross-Sectional Stress Distribution

Figure 7 shows the stress distribution after each pass on cross-sections of the workpiece located at 55 mm, 65 mm, 75 mm, 85 mm, 95 mm, and 105 mm from the fixed end. It can be observed that the stress is higher in the stage when the roller loads the workpiece and before the roller unloads the workpiece. This is due to the fact that in the first half loading section when the roller loads the workpiece, the compound movement of the roller relative to the workpiece and the undeformed area of the workpiece at the 60° corner pull the material between the roller and the undeformed area, leading to the development of tensile stress. In the second half loading stage before the roller unloads the workpiece, the compound movement of the roller and the 300° undeformed area of the workpiece compress the material locally, leading to the development of compressive stress.

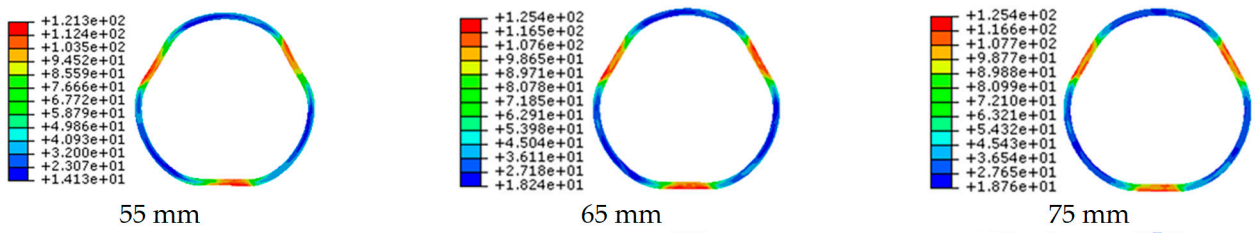


Figure 7. *Cont.*

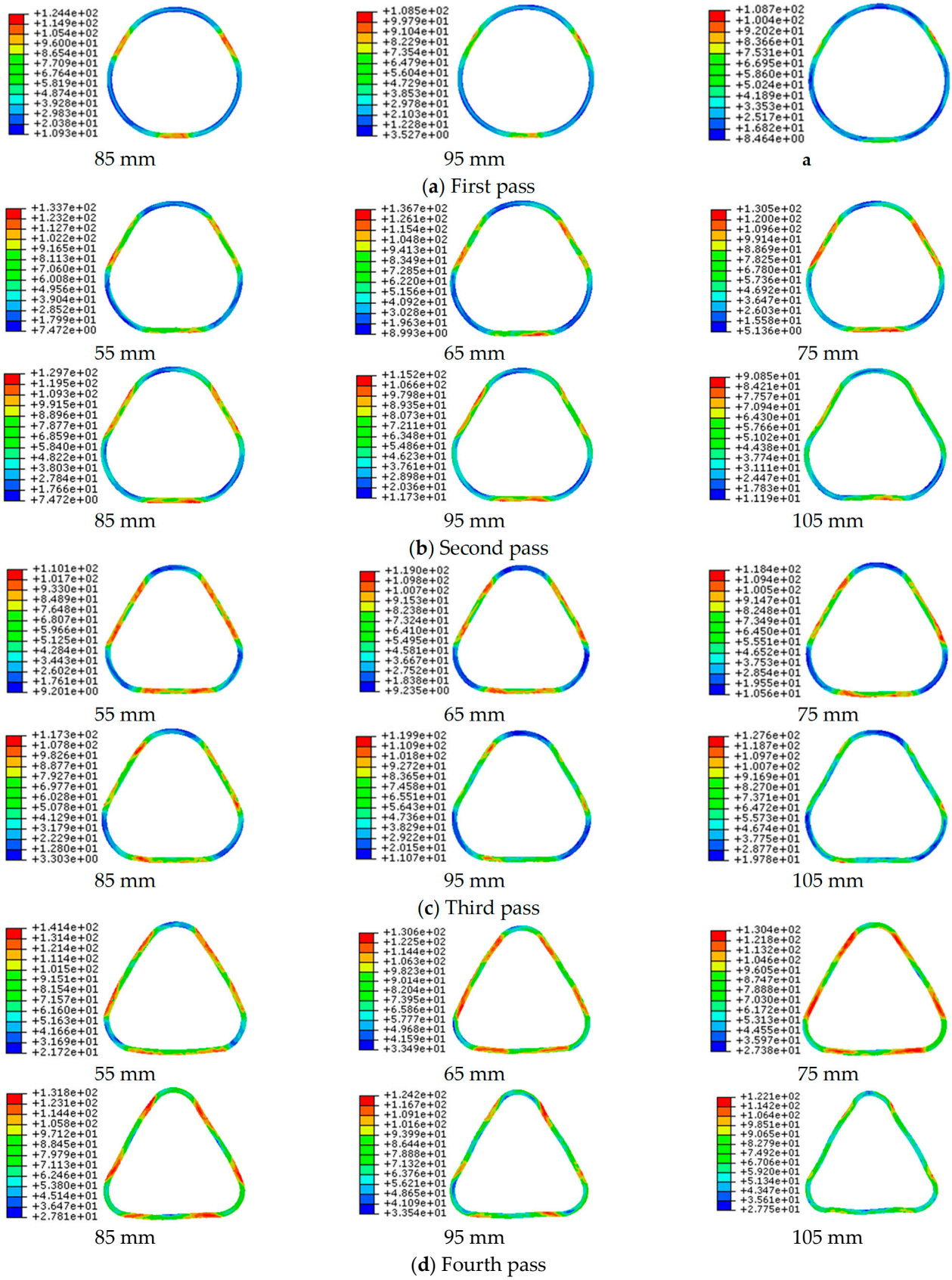


Figure 7. *Cont.*

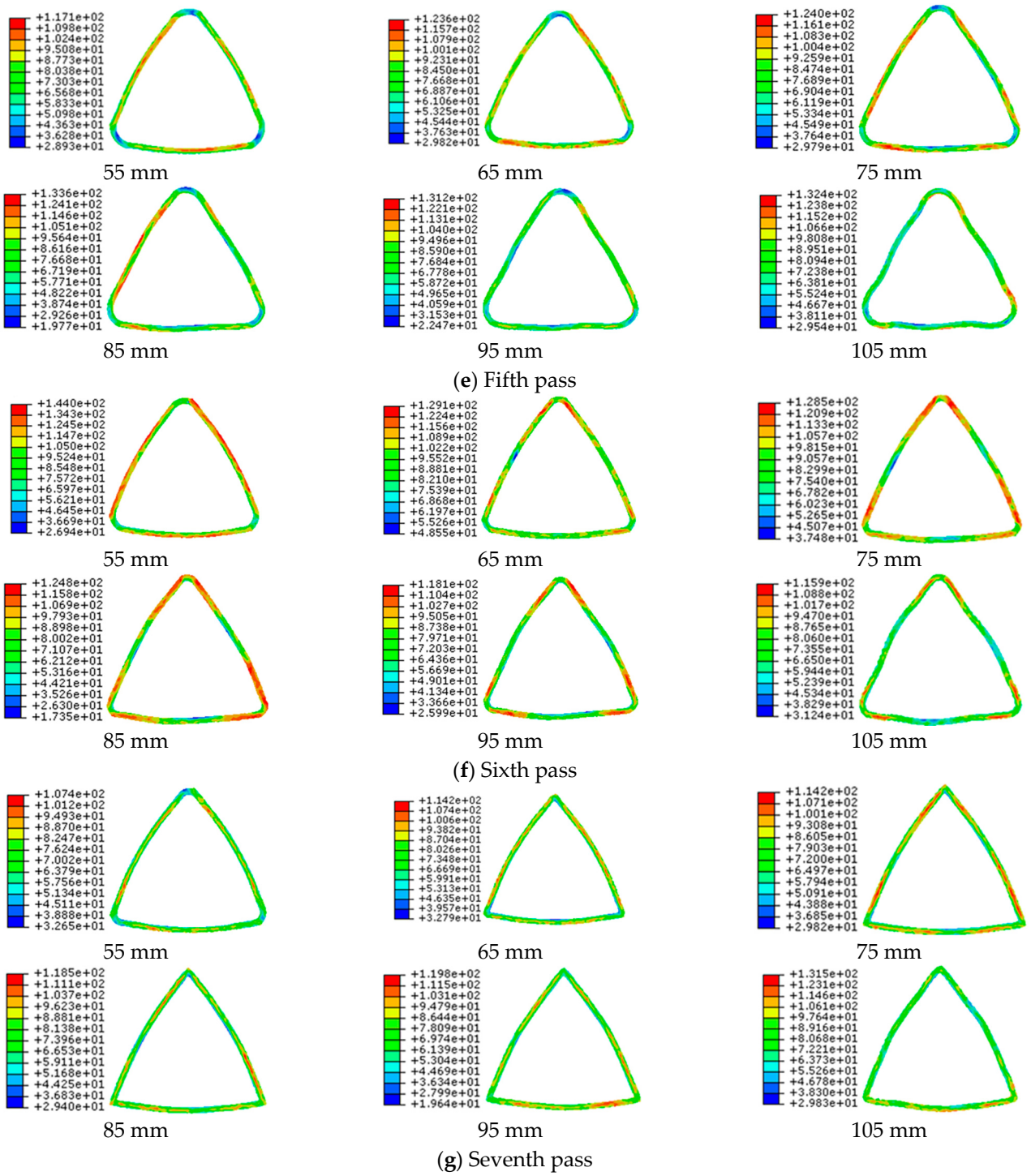


Figure 7. Cross-sectional equivalent von Mises stress distribution after each pass of the trilateral spinning process (MPa).

By comparing the cross-sections at different position after each pass, it can be observed that 65–85 mm is a relatively stable spinning stage, where the cross-section shapes are quite regular. The cross-section profiles at 105 mm (near the free end) after the fifth, sixth, and seventh passes exhibited obvious fluctuations. Due to that, in this experiment, there are 7 spinning passes, after the fifth pass, the work hardening reduces the plasticity of the material, which affects the forming characteristics of the workpiece. At the same time, the 105 mm cross-section is close to the free end. The material in this area

lacks constraints, which results in poor plastic stability and a strong elastic effect. Consequently, the workpiece cannot be fully deformed by the roller; thus, the cross-section profile presents fluctuations.

3.2. Strain Distributions

3.2.1. Equivalent Plastic Strain Distribution

Figure 8 demonstrates the equivalent plastic strain distribution in the workpiece after each pass. It can be observed that after three spinning passes the strain in the workpiece is relatively high where the roller loading acts on the workpiece and before the roller unloading the workpieces, which is in accordance with the stress analysis results. This is due to the fact that during the loading stage, the undeformed area in the 60° corner and the roller pulls the material between them, generating tensile strain. On the other hand, before the unloading stage, the undeformed area in the 300° corner and the roller compresses the material between them, generating compressive strain.

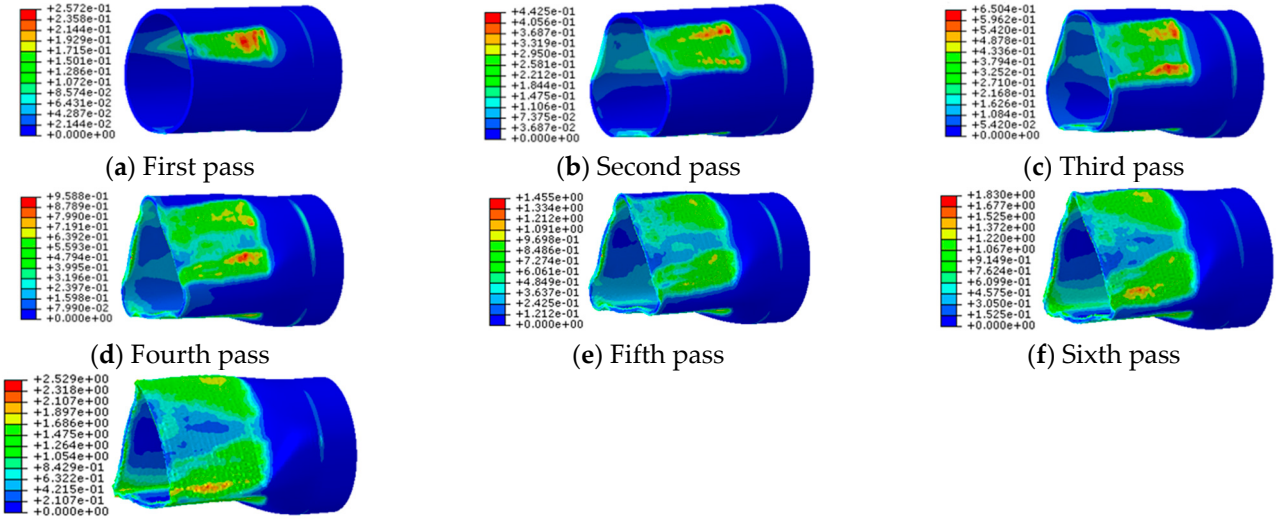


Figure 8. Equivalent strain distribution in the workpiece after each pass of the trilateral spinning process.

3.2.2. Principal Strain Distribution

Figure 9 presents the distribution of three different principal strains in the workpiece after each pass. It can be observed that in the radial direction, the first four passes produce high tensile strain in the areas where the roller starts to perform the forward pass. In this area, the radial feed of the roller and the undeformed area of the workpiece near the fixed end pull the material, resulting in tensile strain. After the 5th, 6th, and 7th passes, in the area where the roller gradually loads the workpiece, the strain in the radial direction is compressive. This is due to that the compound movement of the rollers relative to the workpiece compressing the material along the radial direction when the roller load is on the workpiece. In the area before the roller unloading the workpiece, the workpiece exhibits tensile strain in the radial direction, which is due to the compound movement of the roller pulling the material in the area along the radial direction.

The distribution of the tangential equivalent strain also exhibits a certain trend. After the 5th, 6th, and 7th passes, the area where the roller gradually loads onto the workpiece presents tangential tensile strain. This is attributed to the fact that during the loading stage, the material in this area is stretched from the tangential direction by the roller and the undeformed area of the workpiece at the 60° corner. Additionally, in the area where the roller unloads the workpiece, the workpiece presents compressive strain, which is due to that, during processing the material in this area is compressed by the undeformed area of the

workpiece at the 300° corner and the roller in the tangential direction. Although in the simulation results in this area, no obvious wrinkling was observed. In practice, local wrinkling may be generated due to the presence of negative strain in the tangential direction.

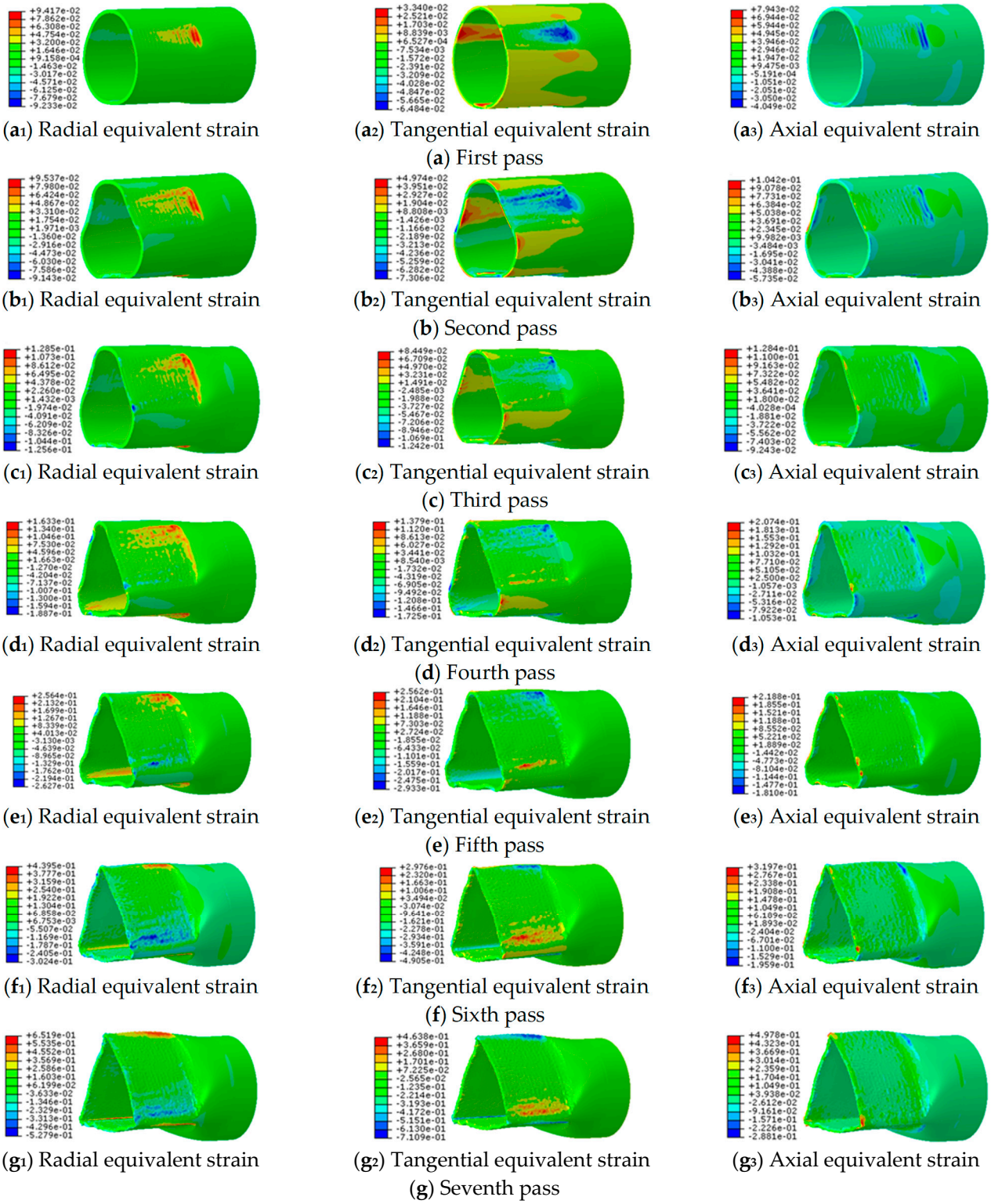


Figure 9. Distribution of the three principal strains in the workpiece after each pass of the trilateral spinning process.

In the axial direction, the workpiece generally presents tensile strain after each pass. Only in the area where the roller starts to perform the forward pass, the workpiece exhibits compressive strain; because when the forward pass begins, the rear part of the roller close to the fixed end compresses the material of the workpiece while restricting its flow. At the end of the backward pass, the roller also compresses the material in this area. Nevertheless, no obvious wrinkling was observed in the negative strain areas in the axial direction.

3.3. Forming Quality Analysis

3.3.1. Wall Thickness Distribution at the 0° Section

Figure 10 shows the wall thickness distribution of the 7 passes along the axial direction at the 0°section of the workpiece. It can be observed that the wall thickness in the range of 65–90 mm from the fixed end is stable, and it is in the stable spinning stage consistent with cross-sectional stress distribution analysis. At the position 55 mm away from the fixed end, the thickness change is large, so necking and fracture may occur here, which is consistent with the stress analysis above. This is attributed to the starting point of the forward pass being located in this area. Although the staggered method has been employed, the cross-section at this position is pulled by the radial feed of the roller and the undeformed part of the workpiece near the fixed end during processing, generating tensile strain and inducing gradual thinning of this area. In addition, the wall thickness near the free end changes a lot due to that the accumulated material at the free end would continue to be pushed out by the roller along the axial direction during the forward pass. Therefore, the thickness of this part is much smaller than in other parts of the workpiece. In general, the thinning rate of the workpiece is about 15%, which is within the acceptable range [1].

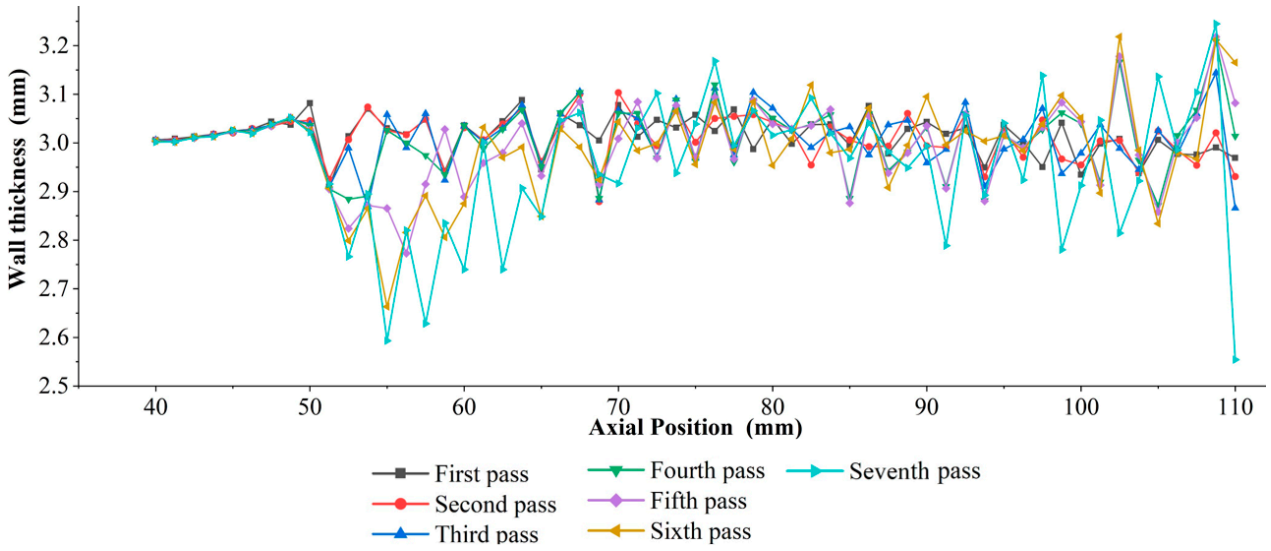


Figure 10. Wall thickness distribution at the 0° section after each pass.

3.3.2. Wall Thickness Distribution at the 60° Section

Figure 11 shows the wall thickness distribution along the tangential direction at the 60° section of the workpiece. It can be observed that the overall wall thickness of this section exhibits a tendency to increase gradually after the first 6 passes. In the 7th pass, the section exhibits a sudden thickening. This is due to that the 60° section is in the transitional area between the newly processed surface and the previously processed surface. Before the roller unloaded the previously processed surface of the workpiece, the roller compresses the 60° section, and material flows to this section, inducing a thickening effect. When the roller gradually loads the newly processed surface, the arc part of the roller which is close to the 60° section extrudes the material and prevents it from flowing along the same direction with the roller. This also increased the thickness of the 60° section. After the 7th

pass, the unloading position of the roller on the previously surface and the loading position of the newly processed surface are very close to the 60° cross-sectional area. Consequently, the thickening effect of the roller on these two processed surfaces acts almost exclusively on the 60° section, and as a result, the thickening effect on the 7th pass is very apparent. Again, the thinning rate of the workpiece is within 15%.

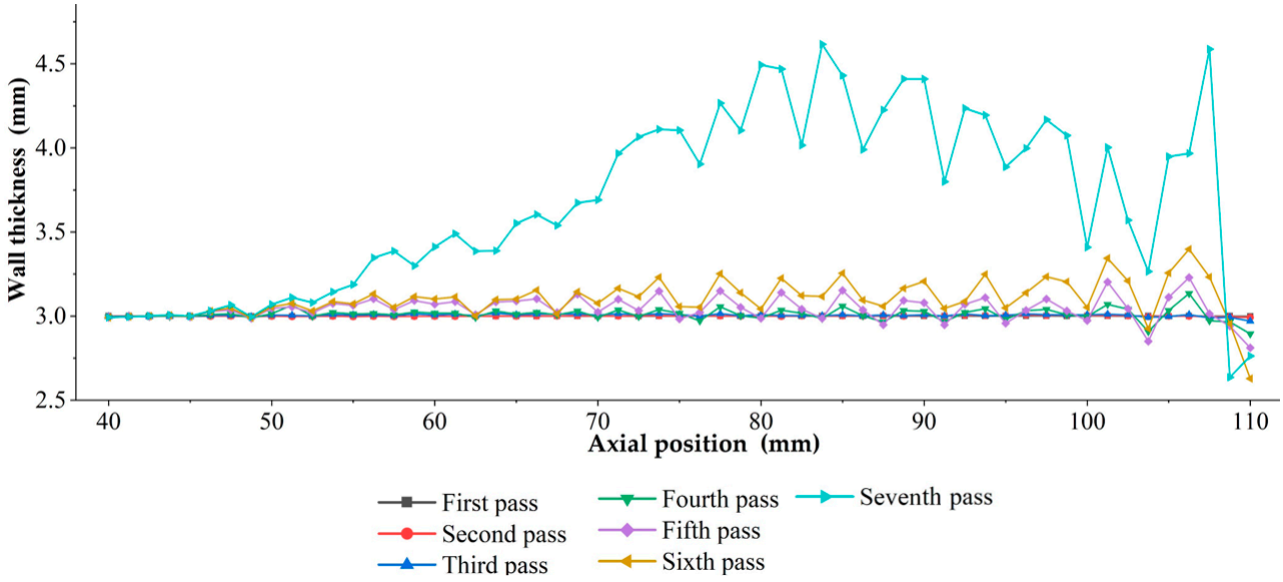


Figure 11. Wall thickness distribution at the 60° section after each pass.

3.3.3. Wall Thickness Distribution at the 55 mm Cross-Section

Figure 12 shows the wall thickness distribution at the 55 mm cross-section of the workpiece. According to the above analysis, the 55 mm cross-section is a vulnerable section, where necking or fracture may occur, leading to the interruption of the spinning process. Therefore, it is necessary to investigate the thickness distribution at the 55 mm cross-section. In Figure 12, the distribution trend of the wall thickness in the tangential direction can be observed. The thinning effect is more significant near the middle of each processing surface, while the thickening effect is more apparent at the corners. This is due to the fact that, during processing, the roller continuously pushes the material from the middle of the surface towards the corners. The overall thinning rate of the cross-section is less than 21%, which is within the acceptable range.

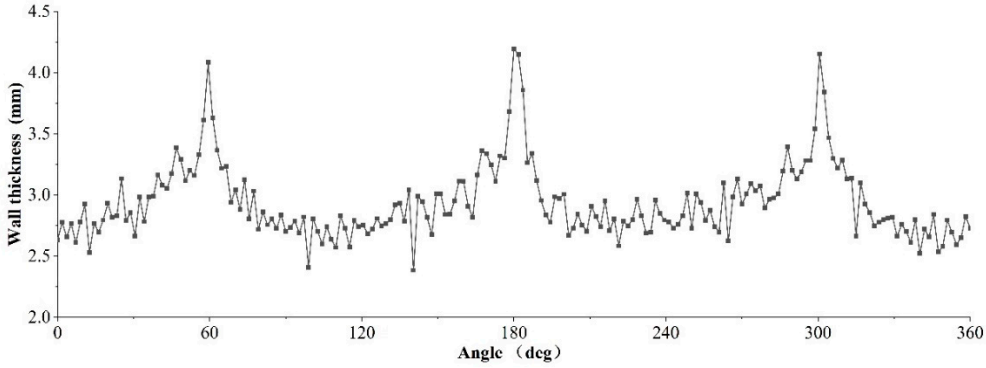


Figure 12. Wall thickness distribution at the 55 mm cross-section.

3.3.4. Wall Thickness Distribution at the 85 mm Cross-Section

Figure 13 shows the wall thickness distribution at the 85 mm cross-section of the workpiece. The section is in the stable spinning stage. It can be observed that the processing

surface near the middle is thinner than the other areas, while a thickening effect can clearly be observed at the corners. However, the overall thinning is lower than that in the 55 mm cross-section, while the overall thickening is higher than that in the 55 mm section. At this section, the thinning rate is less than 15%, which is within the acceptable range.

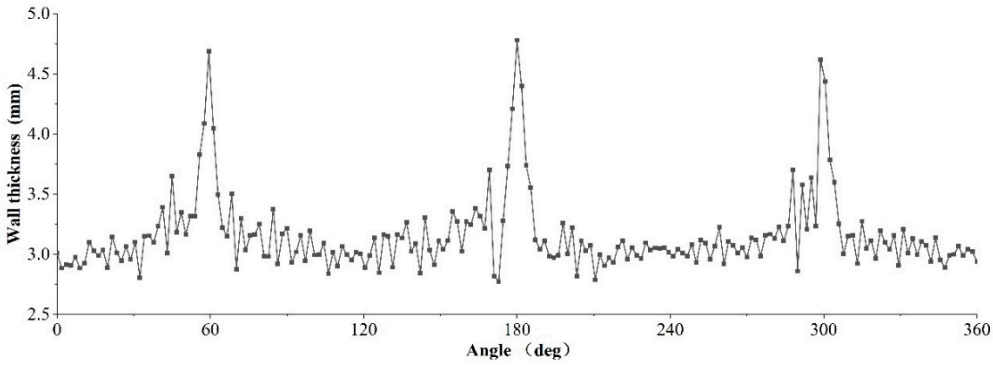


Figure 13. Wall thickness distribution at the 85 mm cross-section.

4. Analysis of Spinning Force

Figure 14 shows the variation of spinning force during the roller loading and unloading the workpiece in each pass. The longest contact time between the roller and the workpiece is 0.007 s. The trend of spinning force is roughly the same for each pass. In the initial loading stage, the spinning force reaches a peak and then decreases. Before the roller unloads, the spinning pressure reaches a peak again.

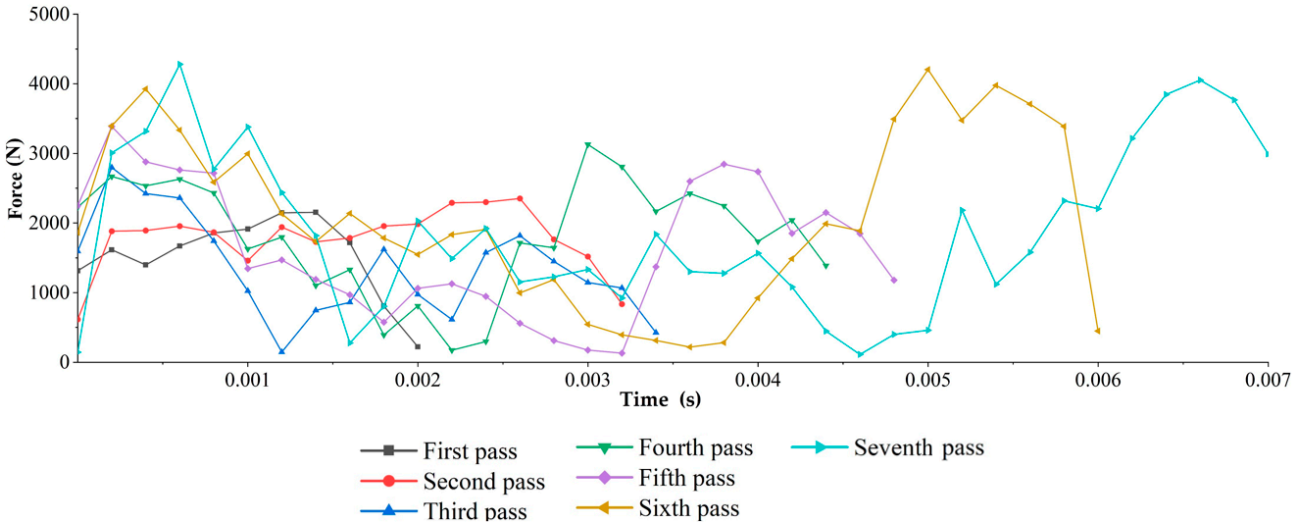


Figure 14. Variation of spinning force with time during.

This trend in consistent with the loading condition between the roller and the workpiece during the spinning process. In the initial roller loading on the workpiece, the roller exerts more and more force to produce the workpiece deformation. After that the spinning force decrease after reaching a peak. That is because the following part of the material already has pre-deformation in the roller initial loading, required less spinning force for its deformation. Then, before the workpiece is unloaded, the movement of the roller relative to the workpiece compressed the materials of the workpiece with the undeformed area of the workpiece at the 300° corner, causing the spinning force to increase again, this produced the second peak of the spinning force. After reaching the second peak, the spinning force decreases due to the separation of the roller and the workpiece.

5. Conclusions

The purpose of this paper was to investigate the feasibility of trilateral non-circular spinning with the theory of concentric circle trajectory. Additionally, the trilateral parts are the maximum deformation that a workpiece with cylinder blank can undergo. In this paper, the trajectory of the roller, as well as the theory of trilateral non-circular spinning, were derived. Moreover, the entire process was simulated, and the simulation results were analyzed. The main conclusions as follows:

A novel method is proposed to process trilateral parts with a high rotational velocity, while ensuring the high accuracy of roller processing trajectory. The efficiency is greatly improved from 60–240 to 600 rpm, the thinning rate is below 21% which is within acceptable limits.

After 7 passes, the starting area of the forward pass exhibits a relatively high von Mises stress magnitude, and it is the most vulnerable area during the spinning process.

In the area where the roller unloads the workpiece and the area where the roller starts the forward pass, local wrinkling may be generated. Though no obvious wrinkles in the negative strain area were observed in the simulation result, these regions need to be paid attention in future practical experiments.

After the completion of the process, the wall thickness distribution at the 55 mm and 85 mm cross-sections demonstrated a consistent trend, where the section near the middle surface is thinner, while a thickening effect is apparent at the corners.

Author Contributions: P.G. and B.W. conceived the conceptualization; X.Z. designed the experiments; X.O. performed the experiments; J.L. and S.Y. analyzed the data; X.O. wrote the paper. All authors have read and agreed to the published version of the manuscript.

Funding: This research was funded by the Jilin Province Development and Reform Commission (2021C038-4), the Science and Technology Development Projects of Jilin Province (20210204143YY), the Science and Technology Development Projects of Changchun (21ZY25), the Scientific research project of Jilin Provincial Department of education in 2021 (JJKH20211078KJ), the Yancheng Intelligent Terminal Industrial Research Institute of Jilin University (JDYCYJY2021-15), the Laboratory and Equipment Management Department of Jilin University (409020720224), the Graduate Innovation Fund of Jilin University (101832020CX112,101832020CX116), the Science and Technology Development Project of Jilin Province (No. 20190302038GX), and the Chongqing Research Institute of Jilin University.

Institutional Review Board Statement: Not applicable.

Informed Consent Statement: Not applicable.

Data Availability Statement: Not applicable.

Conflicts of Interest: The authors declare no conflict of interest.

References

1. Zhang, T. *Spinning Forming Technology*; Chemical Industry Press: Beijing, China, 2019; pp. 1–4.
2. Zeng, R.; Ma, F.; Huang, L.; Li, J.J. Investigation on spinnability of profiled power spinning of aluminum alloy. *Int. J. Adv. Manuf. Technol.* **2015**, *80*, 535–548. [CrossRef]
3. Music, O.; Allwood, J.M.; Kawai, K. A review of the mechanics of metal spinning. *J. Mater. Process. Technol.* **2010**, *210*, 3–23. [CrossRef]
4. Wong, C.C.; Dean, T.A.; Lin, J. A review of spinning, shear forming and flow forming processes. *Int. J. Mach. Tools Manuf.* **2003**, *43*, 1419–1435. [CrossRef]
5. Roy, B.K.; Korkolis, Y.P.; Arai, Y.; Araki, W.; Kouyama, J. Experimental and numerical investigation of deformation characteristics during tube spinning. *Int. J. Adv. Manuf. Technol.* **2020**, *110*, 1851–1867. [CrossRef]
6. Amano, T.; Tamura, K. The study of an elliptical cone spinning by the trial equipment. In Proceedings of the Third International Conference on Rotary Metalworking Processes, Kyoto, Japan, 8–10 September 1984; pp. 213–224.
7. Gao, X.C.; Kang, D.C.; Meng, X.F.; Wu, H.J. Experimental research on a new technology–ellipse spinning. *J. Mater. Process. Technol.* **1999**, *94*, 197–200. [CrossRef]
8. Cheng, Q.K.D. The study of elliptic spinning technique. *J. Plast. Eng.* **1997**, *4*, 56–59.

9. Xia, Q.X.; Zhang, P.; Wu, X.Y.; Cheng, X.Q. Research on distributions of stress and strain during spinning of quadrilateral arc-typed cross-section hollow part. In Proceedings of the International Conference on Mechanical, Industrial, and Manufacturing Engineering, Melbourne, Australia, 15–16 January 2011; pp. 17–20.
10. Xia, Q.X.; Wang, Y.P.; Yuan, N.; Cheng, X.Q. Study on Spinning of Pentagonal Cross-section Hollow-part Based on Orthogonal Experiment Design. In Proceedings of the International Conference on Advanced Design and Manufacturing Engineering (ADME 2011), Guangzhou, China, 16–18 September 2011; pp. 783–788.
11. Xia, Q.X.; Lai, Z.Y.; Long, H.; Cheng, X.Q. A study of the spinning force of hollow parts with triangular cross sections. *Int. J. Adv. Manuf. Technol.* **2013**, *68*, 2461–2470. [CrossRef]
12. Shimizu, I. Asymmetric forming of aluminum sheets by synchronous spinning. *J. Mater. Process. Technol.* **2010**, *210*, 585–592. [CrossRef]
13. Jia, Z.; Han, Z.R.; Xu, Q.; Peng, W.F. Numerical simulation and experiment study on hollow spinning process for square cross-section cone. *Int. J. Adv. Manuf. Technol.* **2014**, *75*, 1605–1612. [CrossRef]
14. Jia, Z.; Han, Z.R.; Xu, Q.; Peng, W.F.; Kong, Q.M. Effects of processing parameters on the surface quality of square section die-less spinning. *Int. J. Adv. Manuf. Technol.* **2015**, *80*, 1689–1700. [CrossRef]
15. Han, Z.R.; Xiao, Y.; Zhou, S.Y.; Jia, Z. Modification of roller path for square cone by die-less asymmetric spinning. *J. Braz. Soc. Mech. Sci. Eng.* **2020**, *42*, 1–9. [CrossRef]
16. Jia, Z.; Fan, Z.J.; Han, Z.R. Study on die-less spinning of square section cone with fillets. *Int. J. Adv. Manuf. Technol.* **2020**, *106*, 5149–5157. [CrossRef]
17. Sugita, Y.; Arai, H. Development of Synchronous Multipath Metal-Spinning Method for Forming Nonaxisymmetric Shapes. *Trans. Jpn. Soc. Mech. Eng. Ser. C* **2012**, *78*, 1004–1012. [CrossRef]
18. Sugita, Y.; Arai, H. Effect of pass-set shape on formability in synchronous multipass spinning. In Proceedings of the 11th International Conference on Technology of Plasticity (ICTP), Nagoya, Japan, 19–24 October 2014; pp. 2373–2378.
19. Sugita, Y.; Arai, H. Formability in synchronous multipass spinning using simple pass set. *J. Mater. Process. Technol.* **2015**, *217*, 336–344. [CrossRef]
20. Härtel, S.; Laue, R. An optimization approach in non-circular spinning. *J. Mater. Process. Technol.* **2016**, *229*, 417–430. [CrossRef]
21. Arai, H.; Kanazawa, T. Synchronous multipass spinning of oblique-bottom shape. *J. Mater. Process. Technol.* **2018**, *260*, 66–76. [CrossRef]
22. Arai, H. Robotic metal spinning–Forming non-axisymmetric products using force control. In Proceedings of the IEEE International Conference on Robotics and Automation (ICRA), Barcelona, Spain, 18–22 April 2005; pp. 2691–2696.
23. Awiszus, B.; Meyer, F. Metal Spinning of Non-Circular Hollow Parts. In Proceedings of the 8th International Conference on Technology of Plasticity, Verona, Italy, 9–13 October 2005; pp. 353–355.
24. Arai, H. Force-controlled metal spinning machine using linear motors. In Proceedings of the IEEE International Conference on Robotics and Automation (ICRA), Orlando, FL, USA, 15–19 May 2006; pp. 4031–4036.
25. Baleanu, D.; Jafari, H.; Khan, H.; Johnston, S.J. Results for Mild Solution of Fractional Coupled Hybrid Boundary Value Problems. *Open Math.* **2015**, *13*, 601–608. [CrossRef]
26. Khan, H.; Alshehri, H.M.; Khan, Z.A. A Fractional-Order Sequential Hybrid System with an Application to a Biological System. *Complexity* **2021**, *2021*, 2018307. [CrossRef]
27. Ullah, I.; Ahmad, S.; Al-Mdallal, Q.; Khan, Z.A.; Khan, H.; Khan, A. Stability analysis of a dynamical model of tuberculosis with incomplete treatment. *Adv. Differ. Equ.* **2020**, *202*. [CrossRef]
28. Xia, Q.; Cheng, X.; Long, H.; Ruan, F. Finite element analysis and experimental investigation on deformation mechanism of non-axisymmetric tube spinning. *Int. J. Adv. Manuf. Technol.* **2012**, *59*, 263–272. [CrossRef]
29. Homberg, W.; Hornjak, D. Friction-spinning of tubular components–Basic research on parameter influence and process design. Special Edition. In Proceedings of the 10th International Conference on Technology of Plasticity, ICTP 2011, Achen, Germany, 25–30 September 2011; pp. 548–553.
30. Ou, X.B.; Zhu, X.Y.; Gu, P.; Wang, B.C.; Li, J.; Liu, X.; Liu, C.; He, F.; Li, Q. Finite Element Analysis and Investigation on Spinning of Quadrilateral Parts with Hollow Cross-Sections Based on Hypocycloid Theory. *Appl. Sci.* **2020**, *10*. [CrossRef]
31. Liu, X.L.; Liu, X.H. Plain motion of hypocycloid. *J. Chang. Railw. Univ.* **1998**, *1*, 75–79. [CrossRef]
32. Xia, H.Y.; Dai, J.P.; Zhao, C. The trajectory property analysis of inner cycloid *Mech. Electr. Eng. Technol.* **2017**, *46*, 25–30.